Thermal relaxation and heat transport in one-dimensional systems: a comparative study

Carlos Olivares[1] and Celia Anteneodo[1]

[1] *Department of Physics, PUC-Rio, Rio de Janeiro, Brazil*

(Dated: June 1, 2017)

By means of molecular dynamics simulations, we analyze the relaxation to equilibrium of one-dimensional systems, after applying a kinetic energy perturbation. We consider systems of rotators, linear and nonlinear oscillators. The relaxation time τ follows a scaling with size N, $\tau \sim N^{\delta}$, where δ depends on the kind of system and energy range. We relate this result with the scaling of the conductivity $\kappa \sim N^{\gamma}$ and discuss this relation with the type of heat diffusion.

PACS numbers: 44.10.+i, 05.60.-k, 05.70.Ln, 66.30.Xj

I. INTRODUCTION

The study of the relaxation of a system towards equilibrium is important to understand the nature of irreversibility and non-equilibrium properties of a system [1–4]. In particular, heat conduction. Even with the enormous efforts to understand non-equilibrium phenomena a general theory is still lacking [5, 6]. Numerical simulations provide an alternative approach, allowing the realization of computer experiments. For instance, by applying reservoirs at different temperatures to a system, or preparing an isolated system with a non-uniform temperature and let it evolve to the equilibrium [7]. A connection between these two approaches is possible, for instance, if the Fourier law is satisfied. In such case, the conductivity must be inversely proportional to the relaxation time of an out-of-equilibrium system [8]. Notwithstanding, Fourier's law is not always satisfied in one-dimensional systems [5, 6, 9] and can present anomalous transport ($\kappa \sim N^a$) [10].

Therefore, the investigation of the connection between relaxation and the thermal conductivity is a relevant issue, that can contribute both to the fundamental basis [11, 12], as well as to practical applications [8, 13].

On the other hand, long-range systems introduce additional difficulties, such as ensemble inequivalence [14]. The relaxation times in long-range systems are typically larger than in short-range ones [15–19].

Motivated by recent works on thermal transport [9, 20, 21], we explore the relaxation times of systems when a system is subjected to large thermal perturbations.

In this paper we consider for four different systems, namely,... when is applied a temperature split protocol with periodic boundary conditions ($q_{N+1} = q_1$).

II. SYSTEMS AND METHODS

We consider one-dimensional model systems, governed by a classical Hamiltonian of the general form

$$\mathcal{H} = \frac{1}{2}\sum_{i=1}^{N} p_i^2 + \mathcal{U}(q_1, \ldots, q_N)\,. \tag{1}$$

yielding the equations of motion:

$$\begin{aligned} \dot{q}_i &= p_i, \qquad \text{for } 1 \le i \le N, \\ \dot{p}_i &= -\frac{\partial \mathcal{U}}{\partial q_i}\,. \end{aligned} \tag{2}$$

Boundary conditions are periodic. We will analyze as particular cases rotators with ferromagnetic-like (either short and long range) couplings, linear oscillators, and non-linear Fermi-Pasta-Ulam-Tsingou springs, as described below.

We consider the $\alpha - XY$ classical rotators [22, 23], a paradigmatic model that allows to control the range of the interactions, whose potential energy is defined as

$$\mathcal{U} = \frac{1}{2\widetilde{N}^{\alpha}} \sum_{i=1}^{N}\sum_{j\neq i}^{N} \frac{\mathcal{V}(q_i - q_j)}{r_{i,j}^{\alpha}}\,, \tag{3}$$

where

$$\mathcal{V}(x) = 1 - \cos x\,, \tag{4}$$

$r_{i,j}$ is the minimal distance between rotators i and j, over the circle of length N, and the normalization factor is

$$\widetilde{N}^{\alpha} \equiv 2\sum_{r=1}^{N/2} r^{-\alpha} = \begin{cases} 2 & \text{if } \alpha \to \infty, \\ N & \text{if } \alpha = 0. \end{cases} \tag{5}$$

We will focus in these extreme cases, that correspond to pairwise nearest-neighbor ($\alpha \to \infty$) and global ($\alpha = 0$) couplings. In the first case, the total potential energy becomes

$$\mathcal{U} = \frac{1}{2}\sum_{i=1}^{N} \mathcal{V}(q_i - q_{i+1})\,. \tag{6}$$

In the latter case, also known in the literature as HMF [24], the total potential energy takes the form

$$\mathcal{U} = \frac{1}{2N}\sum_{i=1}^{N}\sum_{j\neq i}^{N} \mathcal{V}(q_i - q_j)\,. \tag{7}$$

We will also investigate the following simple short range systems, where the interaction energy in Eq. (6) is given by

$$\mathcal{V}(x) = \begin{cases} \frac{x^2}{2} & \text{(HC)}, \\ \frac{x^2}{2} + \frac{x^4}{24} & (\beta\text{-FPUT}), \end{cases} \tag{8}$$

corresponding to chains of harmonic (HC) and anharmonic Fermi-Pasta-Ulam-Tsingou springs (β-FPUT, with $\beta = 1/6$) [25, 26].

Numerical integration of the equations of motion (2) was performed by means of a fourth-order symplectic algorithm [27], with periodic boundary conditions. As initial condition, we set $q_i = 0$ for all i so that all the energy is purely kinetic ($E = K$), and draw the p_i, $i = 1, \ldots, N$ from a uniform distribution. Then, the velocities were shifted, to make the total momentum zero, and scaled to obtain the desired total energy $E = K = NT/2$, where $T = \sum_i^N p_i^2/N$ is the temperature. For each realization, we waited until the isolated system attained equilibrium, identified by the theoretical equilibrium value of the partition between potential and kinetic energies, as well as by the Maxwellian distribution of velocities.

Once at equilibrium, the following perturbation was applied, at a time $t = 0$: we perturbed the system through a kinetic energy split protocol, without affecting the coordinates q_i, and keeping the total energy of the system unchanged. The split protocol consists in defining two subsystems S_h (hot) and S_c (cold), in our case composed by the particles $i = 1, 2, \ldots, N/2$ and $N/2 + 1, \ldots, N$, respectively. The velocities of S_c are set to zero, while the velocities of S_h are scaled by a factor $2T$, in order to exactly compensate the kinetic loss of S_c, after a correction to guarantee zero total momentum. Then, we monitored the relaxation energies of each subsystem, keeping the whole system isolated at the initial total energy E. In all cases we measured average energies over $2^{18}/N$ realizations. Characteristic equilibration times were computed for different sizes N and energies per particle $u = E/N$.

III. RELAXATION BEHAVIOR

A. Short-range XY rotators

Let us start by analyzing the short-range XY model, identified by Eq. (6). This is an exceptional model in the scenario of thermal transport since it is a momentum conserving system with normal heat transport, i.e. finite thermal conductivity [5, 6, 9, 28, 29]. This behavior is attributed to the non-conservation of stretch or the presence of phases (finite and periodic potential energy) [30].

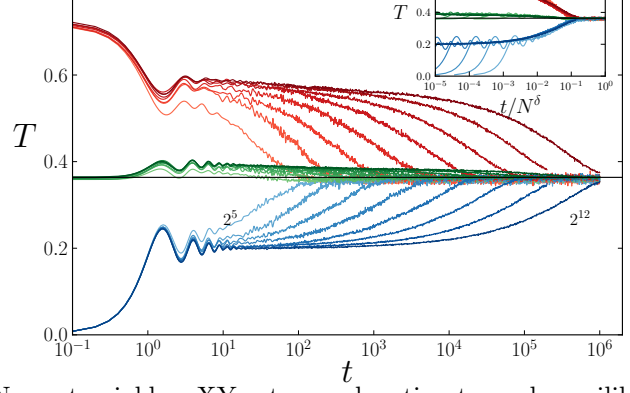

Nearest-neighbor XY rotors: relaxation towards equilibrium, for i

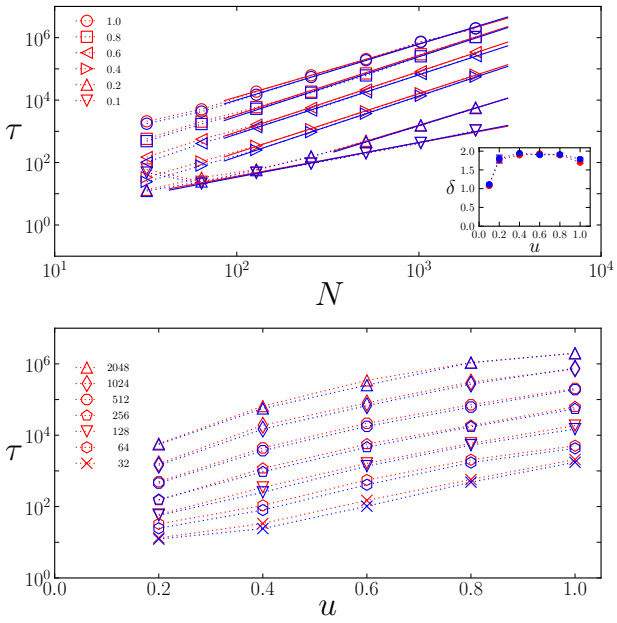

FIG. 1. Nearest-neighbor XY rotors: (a) Relaxation time τ versus system size N for different values of energy u. The solid lines correspond to a power-law fitting with exponents shown in the inset. (b) Relaxation time τ versus u for different values of N. Results for hot and cold subsystems are shown by red and blue symbols respectively.

A representative relaxation portrait after the split protocol is shown in Fig. 1, for energy density $u = 0.4$ and several systems sizes. We represent the (averaged) temperature of each subsystem as well as the temperature of the whole system.

We notice an initial regime of violent relaxation with small oscillations, almost insensitive to system size, followed by a regime of longer duration, that strongly depends on system size. The decay is nearly exponential but instead of obtaining exponential rates from a fitting procedure, we estimated the relaxation time, τ_s, for $s = h, c$ as the time interval required for the temperature difference $\Delta T_s(t) \equiv T_s(t) - T_{eq}$, to fall to 20% of its equilibrium value, T_{eq}, that is $\Delta T_s(\tau_s) = 0.2\Delta T_s(0)$.

The behavior of the relaxation time τ versus N is presented in Fig. 2(a). We observe a scaling behavior N^δ, with values of δ shown in the inset. These values are slightly below 2 for sufficiently large energies per particle u but become close to 1 for $u \lesssim 0.1$. Moreover, τ increases

with u, almost exponentially, as shown in Fig. 2(b).

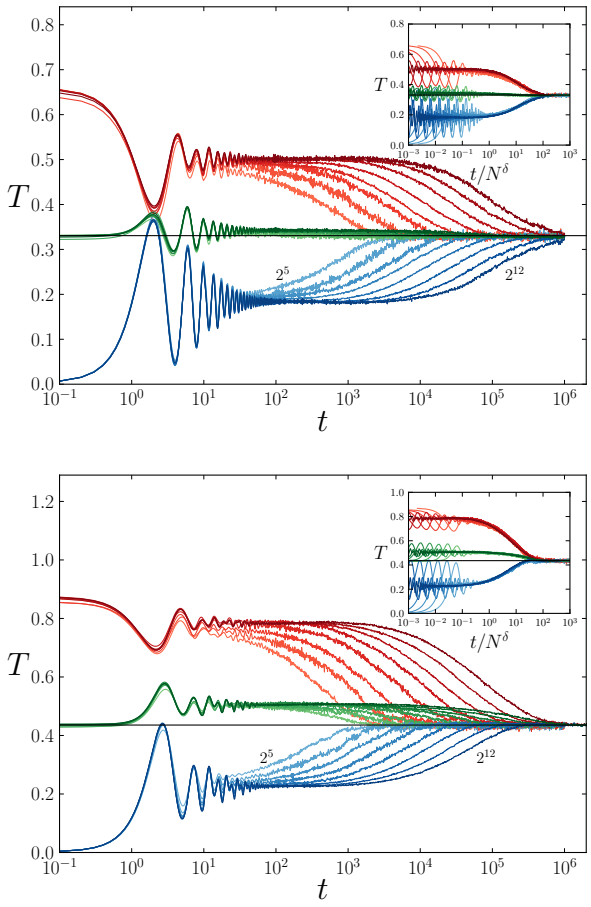

FIG. 2. Mean-field XY rotators: relaxation towards equilibrium for $u = 0.4$ (a) and $u = 0.6$ (b). Temperature of hot (red), cold (blue) subsystems, and whole system (green) versus time t. System sizes are $N = 2^k$, $k = 5, \ldots, 12$. The black horizontal line represents the theoretical equilibrium value. Insets: temperatures versus scaled time t/N^δ, where $\delta = 1.09$ (a) and 1.11 (b).

B. Long-range XY rotators

Now we address the HMF model, identified by Eq. (7). The relaxation of temperatures are shown in Fig.3. Like in the short-range case, we observe a first regime that is independent of system size but with larger oscillations in this long-range case, followed by a size-dependent decay. For $u = 0.4$, Fig.3(a), the profiles are nearly symmetric. For $u = 0.6$, Fig.3(b), there is a noticeable asymmetry and a delay of the cold subsystem with respect to the hot one. These effects are less pronounced at $u = 0.4$ and in the short-range case.

It is worth mentioning, that even if the temperature attained the theoretical equilibrium value, the velocity probability distribution becomes Gaussian at later times, as depicted in Fig. 4, were we plotted the kurtosis versus time. Differently, in the short range case the Gaussian distribution is attained concomitantly with the equilibrium value of the temperature.

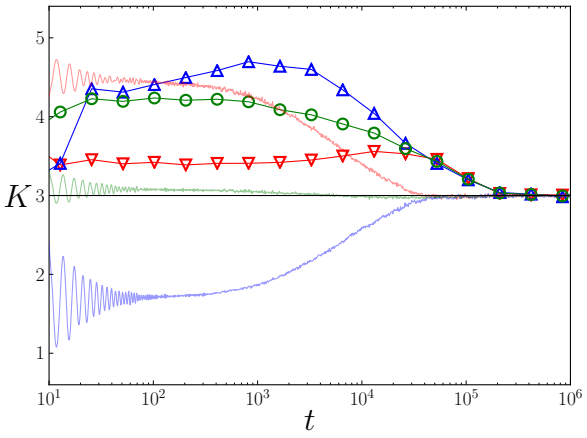

FIG. 3. Temporal evolution of the kurtosis of the velocity distribution of mean-field XY rotators, for $N = 256$ and $u = 0.4$. The solid line corresponds to the Gaussian value $k_4 = 3$, drawn for comparison.

The behavior of the relaxation time versus N is presented in Fig. 5(a)-(b). The relaxation time increases with N following approximately the scaling behavior $\tau \sim N$. Furthermore, the symmetry of the profiles observed for small energies [e.g. $u = 0.4$ in Fig. 3(a)] is reflected in nearly coincident relaxation times. However, for higher energies, the asymmetry [e.g. $u = 0.6$ in Fig. 3(b)] is related to the shorter relaxation times of the cold subsystems.

The dependency of τ on the energy is depicted in Fig. 5(c) for two different system sizes. In contrast to the short-range case, τ does not increase monotonically with u, but presents a minimum value near the critical energy ($u = 0.75$) at which a continuous ferromagnetic transition occurs [22]. In this region there is also enhanced dependency on the system size.

C. Oscillators

In order shed some light on the found scaling laws, we investigate the linear and nonlinear oscillators given by Eq. (**??**).

In the purely harmonic case, the temporal evolution of T is shown in Fig. 6 for $u = 0.4$ and different system sizes. Despite the noisy profiles, probably related to the lack of interaction between modes, the scaling behavior is neatly $\tau \propto N$, that is, $\delta = 1$. Moreover, we observed that this scaling exponent is energy independent, differently to the previous cases.

This scaling law explains the change of behavior observed in the plots of τ versus N, in the short-range XY

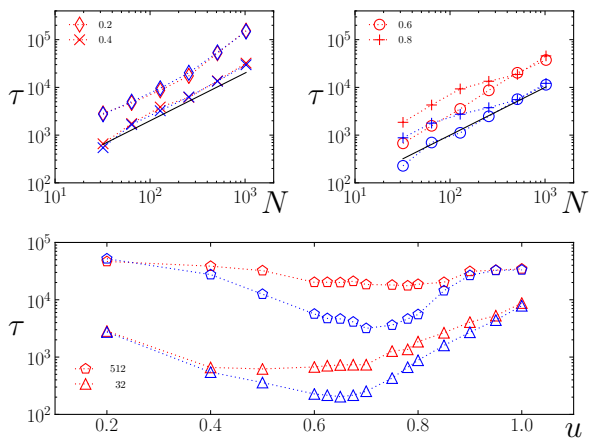

FIG. 4. Mean-field XY rotators: relaxation time τ as a function of system size N for different values of energy u (a)-(b). The solid lines have slope 1, drawn for comparison. Relaxation time as a function of u, for two different system sizes (c). Results for the hot and cold subsystems are shown by red and blue symbols respectively. In all cases averages over $2^{18}/N$ realizations are shown.

case at low energy (see Fig. 2). In fact, at low energies, the rotors feel the nearly harmonic bottom of the potential well, reaching the limit of harmonic oscillators.

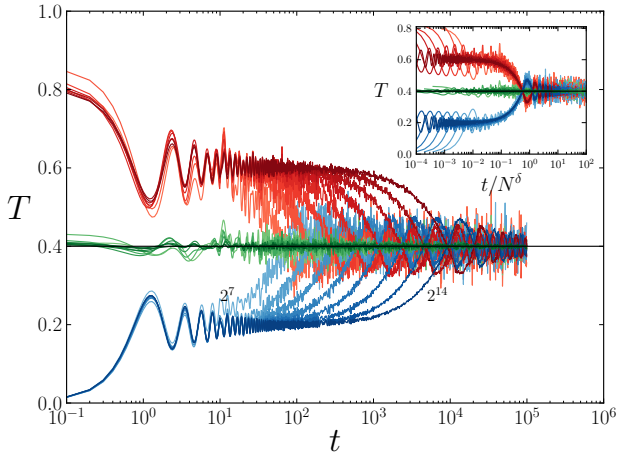

FIG. 5. Harmonic chain: relaxation to equilibrium, as in previous figures, with $u = 0.4$, for sizes $N = 2^k$ for $k = 7\ldots, 14$. The inset shows the scaled data, with $\delta = 1$.

Finally, we investigate the effect of nonlinearities, such as those introduced by the β-FPUT interaction potential, largely studied over the past 60 years [25, 26].

In Fig. 7, we show representative equilibration profiles for the β-FPUT, of different sizes. We found a time scaling factor t/N^δ, where $\delta \simeq 1.68$ for $u = 0.4$ (see inset Fig. 7). This value of δ was obtained by fitting the exponential law $\Delta T_s(t) \sim \exp(-t/\tau)$ at the final stages of equilibration, for sizes $N > 1024$, when large oscillations around the equilibrium temperature are absent. The time scale t/N^δ collapse is shown in the inset, for $\delta = 1.68$.

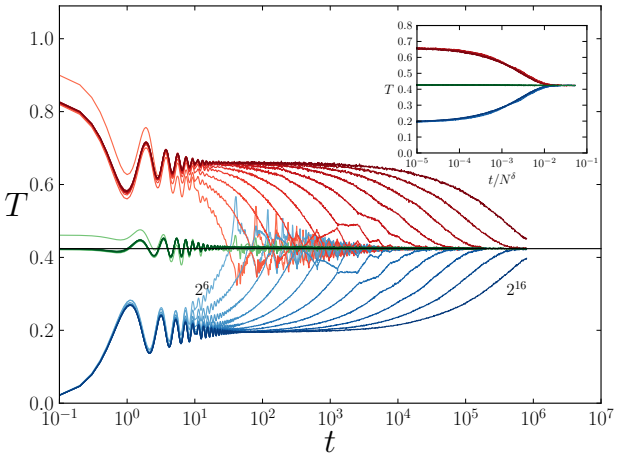

FIG. 6. FPUT oscillators with $\beta = 1/6$: relaxation to equilibrium, for $u = 0.4$, and sizes $N = 2^k$ for $k = 6, \ldots 16$. The scaling collapse is shown in the inset, using $\delta = 1.68$ for $N > 2^{13}$.

In Fig. 8, we show the scaling behavior os the oscillator systems.

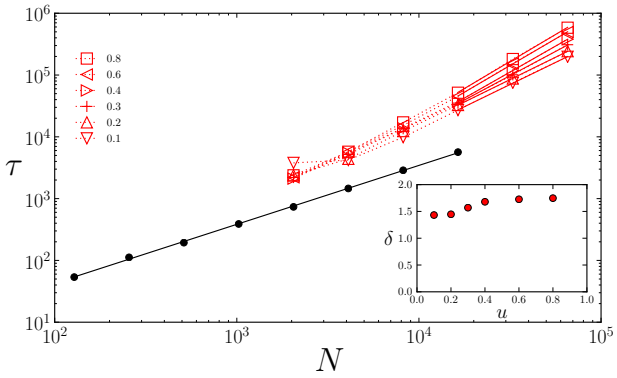

FIG. 7. Oscillators: relaxation time τ versus N, for different values of u. The small filled circles correspond to the chain of harmonic oscillators ($u = 0.4$), the full line has slope $\delta = 1$. While the open symbols correspond to the FPUT chain at the energies indicated on the figures. The inset shows the scaling exponent for the FPUT systems as a function of u.

IV. FINAL COMMENTS

In Fig. 9, we present a comparison of the short and long-range XY systems, showing that the relaxation is slower in the former case, with a larger scaling exponent, for the applied perturbation. While, for the long-range

case the scaling is linear, $\tau \sim N$, for short-range rotators, the scaling is nearly $\tau \sim N^2$, at not too low energies, while also in this case the τ scaling is linear for very low energies. In fact, this is the law observed for linear oscillators. Why long-range rotators behave as linear oscillators is not clear.....

In a recent work, Bagchi and Tsallis investigated a long-range version of the β-FPUT [18], finding a scaling $\tau \sim N^{1.8}$. Although the perturbation is different, the main source of discrepancy may come from the fact that the interaction between subsystems is short-range. Perhaps this is the reason why the scaling is closer to our short-range value, despite the subsystems are long-range.

Moreover, in the long-range XY, at energies near the phase transition critical value $u = 0.75$, the relaxation times are asymmetric. The cold subsystem reaches equilibrium before the hot one for high energies. Moreover, even when equilibrium values have been attained in average, the distribution of velocities becomes Gaussian later.

Another contribution of this work is that even that the for the nearest neighbor rotators the system has a finite thermal conductivity the system does not have the scaling law expected for the relaxation to the equilibrium law behavior.

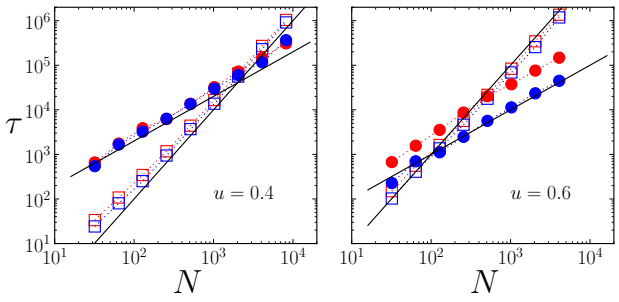

FIG. 8. τ vs N for the short (square) and long (circle) range XY rotators, with energy densities $u = 0.4$ (left) and $u = 0.6$ (right). The red and blue symbols are for the hot and cold subsystems respectively. The black solid line $\tau \sim N$ and N^2 are drawn for comparison.

V. TO ADD IN THE BODY SPREAD OF A PERTURBATION IN THE RING

In order to analyze the spread of the energy in the systems (8), we apply a kinetic perturbation to the two central particles of the system[31]. This perturbation consists in change the kinetic energy of the two central particles to the twice the value of the equilibrium kinetic energy, in opposite directions. Then the momentums of the rest of the particles are corrected to preserve the kinetic energy and total momentum of all the system.

Acknowledgments: We thank Brazilian agencies CNPq and Faperj for partial financial support.

[1] M. Kardar, *Statistical Physics of Particles* (Cambridge University Press, 2007).
[2] K. Huang, *Statistical mechanics* (Wiley, 1987).
[3] M. Toda, R. Kubo, N. Saitō, and N. Hashitsume, *Statistical Physics II: Nonequilibrium Statistical Mechanics*, Series C, English Authors (Springer Berlin Heidelberg, 1992).
[4] G. Gallavotti, W. Reiter, and J. Yngvason, *Boltzmann's Legacy*, ESI lectures in mathematics and physics (European Mathematical Society, 2008).
[5] A. Dhar, Advances in Physics **57**, 457 (2008).
[6] S. Lepri, R. Livi, and A. Politi, Physics Reports **377**, 1 (2003).
[7] F. Bonetto, J. L. Lebowitz, and L. Rey-Bellet, *Mathematical Physics 2000*, , 128 (2000), 0002052 [math-ph].
[8] E. Lampin, P. L. Palla, P.-A. Francioso, and F. Cleri, Journal of Applied Physics **114**, 033525 (2013).
[9] C. Olivares and C. Anteneodo, Phys. Rev. E **94**, 1 (2016).
[10] T. c. v. Prosen and D. K. Campbell, Phys. Rev. Lett. **84**, 2857 (2000).
[11] S. Lepri, Phys. Rev. E **58**, 7165 (1998).
[12] O. V. Gendelman and A. V. Savin, Phys. Rev. E **81**, 020103 (2010).
[13] H. Zaoui, P. L. Palla, F. Cleri, and E. Lampin, Phys. Rev. B **94**, 054304 (2016).
[14] J. Barré, D. Mukamel, and S. Ruffo, Phys. Rev. Lett. **87**, 030601 (2001).
[15] D. Mukamel, S. Ruffo, and N. Schreiber, Phys. Rev. Lett. **95**, 240604 (2005).
[16] G. Miloshevich, J.-P. Nguenang, T. Dauxois, R. Khomeriki, and S. Ruffo, Phys. Rev. E **91**, 032927 (2015).
[17] F. L. Antunes, F. P. C. Benetti, R. Pakter, and Y. Levin, Phys. Rev. E **92**, 052123 (2015).
[18] D. Bagchi and C. Tsallis, Physics Letters A **381**, 1123 (2017).
[19] T. N. Teles, S. Gupta, P. Di Cintio, and L. Casetti, Phys. Rev. E **92**, 020101 (2015).
[20] D. Bagchi, Phys. Rev. E **95**, 032102 (2017).
[21] E. Pereira and R. R. Ávila, Phys. Rev. E **88**, 032139 (2013).
[22] C. Anteneodo and C. Tsallis, Phys. Rev. Lett. **80**, 5313 (1998).
[23] F. Tamarit and C. Anteneodo, Phys. Rev. Lett. **84**, 208 (2000).
[24] M. Antoni and S. Ruffo, Phys. Rev. E **52**, 2361 (1995).

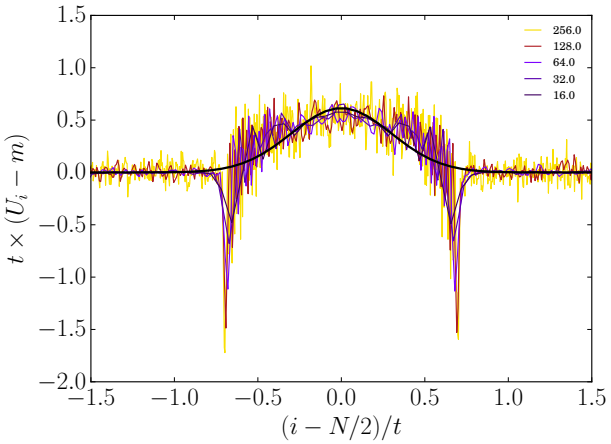

FIG. 9. Time scaled evolution of the energy profile (kinetic and potential) under a perturbation in the middle of the ring, for harmonic potential (HC) with $u = 0.4$ and $N = 1024$. The black line is a fitted Gaussian curve and m is the mean energy of 20 particles at the other side of the ring.

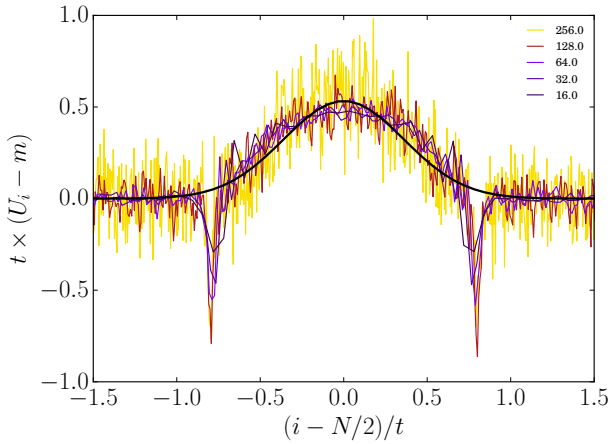

FIG. 10. Time scaled evolution of the energy profile (kinetic and potential) under a perturbation in the middle of the ring, for the FPUT-β system with $u = 0.4$ and $N = 1024$. The black line is a fitted Gaussian curve and m is the mean energy of 20 particles at the other side of the ring.

[25] G. P. Berman and F. M. Izrailev, Chaos: An Interdisciplinary Journal of Nonlinear Science **15**, 015104 (2005).
[26] T. Dauxois, Physics Today **61**, 55 (2008).
[27] H. Yoshida, Physics Letters A **150**, 262 (1990).
[28] C. Giardinà, R. Livi, A. Politi, and M. Vassalli, Phys. Rev. Lett. **84**, 2144 (2000).
[29] O. V. Gendelman and A. V. Savin, Phys. Rev. Lett. **84**, 2381 (2000).
[30] S. G. Das and A. Dhar, (2015), arXiv:arXiv:1411.5247v2.
[31] Due to the periodic boundary conditions the central particles could be any contiguous particles.

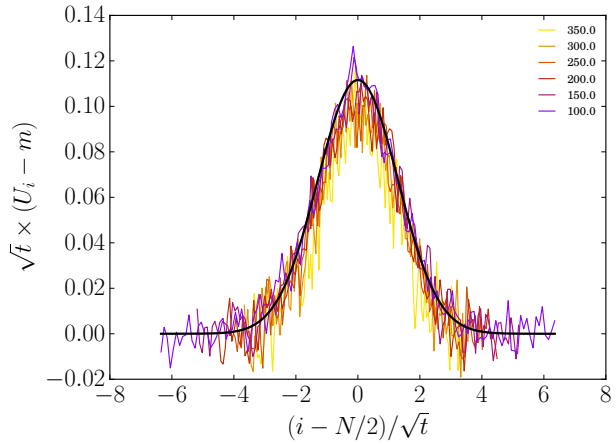

FIG. 11. Time scaled evolution of the energy profile (kinetic and potential) under a perturbation in the middle of the ring, for the XY system with $u = 0.4$ and $N = 128$. The black line is a fitted Gaussian curve and m is the mean energy of 20 particles at the other side of the ring.